$$2\pi(d_{xz/yz} - p_{x/y}(O))^2$$

$$2\sigma(s - d_{z^2} - p_z(O))^2$$

$$1\delta(d_{x^2-y^2/xy})^4$$

$$1\pi(d_{xz/yz} + p_{x/y}(O))^4$$

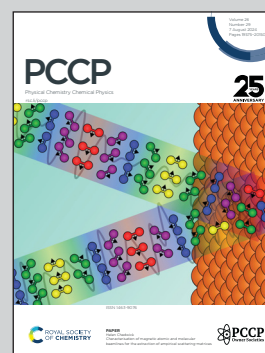$$1\sigma(s + d_{z^2} - p_z(O))^2$$

Ni—O

Energy

Showcasing research from Professor David Dixon's laboratory, Department of Chemistry & Biochemistry, The University of Alabama, USA.

The electronic structure of diatomic nickel oxide

The electronic structure of diatomic NiO using CASSCF, icMRCI+Q, CCSD(T), and DFT was predicted. There is significant ionic character with the $2p_z$ of O forming a σ bond with the $4s/3d_{z^2}$ of the Ni. It is difficult to calculate the vibrational frequency but icMRCI+Q provides a reliable value. The calculated FPD bond dissociation energy is in good agreement with the lower experimental value. 43 DFT functionals were benchmarked to provide guidance for describing more complex NiO systems with only 3 functionals predicting the frequency correctly.

Background credit: Power station by Petmal *via* iStock

ROYAL SOCIETY OF CHEMISTRY

rsc.li/pccp

Registered charity number: 207890

PCCP Owner Societies

Check for updates

The electronic structure of diatomic nickel oxide†

Nickolas A. Joyner, João Gabriel Farias Romeu, [ID] Brian Kent and
David A. Dixon [ID] *

The nature of the Ni–O bond is relevant to catalytic and environmental applications. The vibrational frequency and electronic structure of NiO were calculated using CASSCF, icMRCI+Q, CCSD(T), and DFT. CASSCF predicted a quintet state ($^5\Sigma^-$) ground state for the equilibrium bond distance with a state crossing at 1.65 Å, where the triplet ($^3\Sigma^-$) state becomes of lower energy. These states arise from the $3d^8(^3F)4s^2$ (^3F) and $3d^9(^2D)4s^1$ (^3D) configurations of Ni. The icMRCI+Q method predicts a triplet ($^3\Sigma^-$) ground state and does not predict a state crossing with the quintet. This state has significant ionic character with the $2p_z$ of O bonding with the $4s/3d_{z^2}$ of the Ni to form a σ bond. The NiO frequency at the icMRCI+Q level of 835.0 cm^{-1} is in excellent agreement with experiment; the value of r_e is 1.5992 Å at this computational level. CCSD(T) predicts ω_e = 888.80 cm^{-1} when extrapolated to the complete basis set limit. Frequencies predicted using CCSD(T) deviate from experiment consistent with the calculations showing large multireference character. A wide array of density functionals were benchmarked. Of the 43 functionals tested, the ones that gave the best prediction of the frequency are ωB97XD, CAM-B3LYP, and τ-HCTH with respective values of 831.8, 838.3, and 837.4 cm^{-1} respectively. The bond dissociation energy (BDE) of NiO is predicted to be 352.4 kJ mol^{-1} at the Feller–Peterson–Dixon (FPD) level in good agreement with one of the experimental values. The calculated BDEs at the DFT level are sensitive to the choice of functional and atomic asymptote. Sixteen functionals predicted the BDE within 20 kJ mol^{-1} of the FPD value.

Introduction

Solid oxide electrocatalysts (SOEC) have been a focus in recent years due to their applications in renewable energy conversion and storage,[1] as SOEC catalysts can selectively reduce H_2O and CO_2 to achieve carbon neutral H_2 generation.[2–7] However, with such common Ni-based catalysts, CO_2 reduction is challenging.[8] To increase the efficiency and success of these catalysts, Ni supported on yttria stabilized zirconia (YSZ) is being developed as an SOEC catalyst that can reduce CO_2 with minimal challenges. To fine tune the Ni cathode, a wide array of Ni alloys and NiO materials have been proposed, which require further exploration to understand what role these complexes play in CO_2 reduction.[9–11] It has been established that Ni clusters on YSZ can interact with the oxygens leading to the formation of Ni–O bonds in the solid state. The current goal is to provide insights into the nature of the Ni–O bond by examining diatomic NiO.

There have been several computational and experimental studies of diatomic NiO. However, different values have been

obtained for the vibrational frequencies as shown in Table 1. Ram and Bernath used Fourier transform infrared emission spectroscopy of the A $^3\Pi$–X $^3\Sigma^-$ band of NiO in the near-infrared region and determined the spectroscopic constants for the ground (X $^3\Sigma^-$) and excited (A $^3\Pi$) states by analyzing the vibration–rotation bands.[12] For the ground state, they chose the values of ω_e and $\omega_e x_e$ obtained by Srdanov and Harris in a laser-induced fluorescence (LIF) study including a rotational analysis of NiO.[13] Green *et al.*[14] measured the values of ω_e and $\omega_e x_e$ for NiO in an Ar matrix at 14 K and found similar values to the gas phase spectroscopic values.[13] Anion photoelectron spectroscopy experiments on NiO$^-$ by Wu *et al.*[15] provided the adiabatic electron affinity (AEA) and harmonic vibrational frequency for the ground state of NiO. The ionization energy (IE) and other thermochemical data of NiO were reported by Watson *et al.*[16] in their high-temperature mass spectrometry experiments. Other experimental work on NiO includes the microwave spectrum of pure rotational transitions of the $v = 0$ and $v = 1$ vibrational states,[17] photoelectron spectroscopy of NiO and NiO$^-$,[18] and chemiluminescent reactions of nickel with ozone and measured by mass spectrometry.[19] Farber and Srivastava studied the vaporization of NiO(s) and the thermodynamics of reactions of nickel metal with oxygen vapor using effusion-mass spectrometric to obtain a NiO(g) dissociation

The University of Alabama, Department of Chemistry and Biochemistry, Shelby Hall, Tuscaloosa AL, 35487-0336, USA. E-mail: Dixondadixon@ua.edu

Table 1 Ground state spectroscopic parameters of NiO

Method	r_e (Å)	ω_e (cm^{-1})	D_0 (kJ mol^{-1})	Ref.
Experiment	1.62712			12
Experiment		800(50)		15
Experiment	1.627	839.1 ± 0.5 ($\omega_e x_e$ = 5.4 ± 0.5)		13
Experiment		837.61 ± 1.1 ($\omega_e x_e$ = 5.92 ± 0.6)		14
Experiment			349.4 ± 6.3	20
Experiment			373 ± 3366 ± 30	16
GVB-CI	1.60	841	376	22
CISD	1.608	906	149	23
CISD+Q	1.591	848	254	23
MRCI	1.70	700		24
MRCI+Q	1.67	690		24
ICACPF	1.626	850	362	26
DFT/CAM-B3LYP	1.647	838.3	214.2 (BDE(1))	Current
DFT/τ-HCTH	1.621	837.4	477.6 (BDE(1))	Current
DFT/ωB97XD	1.652	831.8	238.7 (BDE(1))	Current
CCSD(T)/CBS	1.6238	872.1	352.4	Current
icMRCI+Q/CBS	1.5992	835.0	387.7	Current

energy.[20] A lower limit to the dissociation energy of 250.9 ± 19.3 kJ mol^{-1} was reported by Fisher and Armentrout based on reactions of nickel ions with cyclopropane and ethylene oxide using guided ion beam mass spectrometry.[21]

Computational studies of NiO range from density functional theory (DFT), Hartree–Fock, configuration interaction singles and doubles (CISD), and generalized valence bond (GVB) methods. Walch and Goddard used the GVB method to describe the Ni–O bonds in NiO, Ni_2O, Ni_3O, Ni_4O, Ni_4O^+, Ni_5O, and Ni_5O^+.[22] Dolg et al. calculated some of the spectroscopic parameters and binding energies of NiO using ab initio methodologies (SCF, CISD and CISD+Q) with single-electron fit (SEFIT) pseudopotentials and an active space comprising the 4s and 3d Ni atomic orbitals and 2s and 2p O orbitals.[23] The predicted values of the bond distance and ω_e were highly dependent on the computational methodology. Similar behavior was found by Bauschlicher et al.[24] who compared the results from SCF, CISD, CISD+Q, MRCI, and MRCI+Q calculations. These authors noted that the large differences between the CISD and CISD+Q results show that the reference space must be larger, so that multireference CI (MRCI) calculations are necessary. They also disagreed with the description of the bonding by Walch and Goddard III, who predicted that NiO has a covalent bond.[19,21] DFT/B3LYP calculations of NiO have also been reported.[25] Bauschlicher and Maitre[26] have surveyed computational studies of all of the first-row transition metal oxides. They note that it is difficult to calculate the properties of NiO from single reference starting points due to localization of π^* singly occupied orbitals on the Ni or O. Their best values were obtained at the CASSCF/ICACPF (internally contracted average coupled pair functional) level with an extended polarized double-ζ basis set on Ni and the aug-cc-pVTZ basis set on the O without the diffuse f.

Computational methods

The equilibrium geometry (r_e) of NiO was initially optimized using DFT with the hybrid B3LYP exchange correlation functional[27–29] the correlation consistent aug-cc-PVDZ basis set for O,[30,31] and the aug-cc-pVDZ-PP basis set with an effective core potential[32] for Ni.[33,34] The B3LYP geometries were used as starting points for calculations at the CCSD(T) level (coupled cluster theory with single and double excitations with perturbative triples).[35–41] All coupled cluster calculations were performed with the R/UCCSD(T) approach, where the restricted open-shell Hartree–Fock calculation is performed followed by a relaxation of the spin constraint at the coupled cluster level. The CCSD(T) calculations utilized the third-order Douglas–Kroll–Hess Hamiltonian (DKH3), with the aug-cc-pVNZ-DK[42] basis set for O and Ni. This combination of basis sets will be further denoted as aN-DK. Harmonic and anharmonic frequencies (ω_e, $\omega_e x_e$) were obtained using a Dunham expansion at the CCSD(T) level.[43]

The state-averaged complete active space self-consistent field (SA-CASSCF)[44–48] approach was performed to account for non-dynamical correlation effects and describe the lowest spin-free states, ΛS. To account for the two quasi-degenerate ^3F_g and ^3D_g atomic states of Ni coupling with the $O(^3P_g)$ and to improve the convergence near the equilibrium bond distance, 36 ΛS singlet, 37 ΛS triplet, and 39 ΛS quintet states were optimized in the SA-CASSCF calculations. The atomic aug-cc-pVQZ-DK[42] basis set for O and aug-cc-pwCVQZ-DK[49] basis set for Ni were used, and this combination will be denoted as awQ-DK. These calculations were carried out in the highest Abelian point group available, C_{2v}. Expectation values of L_z^2 were calculated to ensure that both degenerate components of each Λ state were correctly accounted for. The active space of NiO includes 14 electrons in nine orbitals (4 × a_1, 2 × b_1, 2 × b_2, 1 × a_2 in C_{2v} symmetry), which have dominant 2p of O and 4s and 3d of Ni.

Dynamic correlation effects were accounted for by using the internally contracted multireference configuration interaction (icMRCI) method taking the SA-CASSCF wavefunctions as a reference, as implemented in MOLPRO.[50–52] The relaxed Davidson correction (+Q)[53] was included as an estimate of missing quadruple excitations. Only the ground state ($^3\Sigma^-$) was optimized and a potential energy curve (PEC) was calculated around the bond distance but keeping the nine A_2 ΛS triplet states as a reference. The same approach was done using second-order perturbation theory (CASPT2)[54,55] in order to recover dynamical correlation effects; however, some points on the ground state

PEC did not fit on the curve well enough to calculate the vibrational properties. The harmonic, and anharmonic frequencies (ω_e, $\omega_e x_e$) were obtained using a Durham expansion[43] in the same interval used in the UCCSD(T)/aD-DK calculation, but at the icMRCI+Q/awQ-DK level. Certain points did not fall on the curves and were not included in the calculation of the frequencies. Inclusion of these points resulted in a large sum of squares of residuals in the fitting procedure, a large deviation in the fitted minimum energy, and yielded a value of $\omega_e x_e > 15$ cm^{-1}. For the icMRCI+Q calculation, even small errors in the energies used in the fit had a significant impact on the predicted $\omega_e x_e$ for the ground state. Thus, only ω_e was calculated from the fit for the icMRCI+Q. Spectroscopic properties produced by the CASSCF, icMRCI+Q, and CCSD(T) calculations were then extrapolated to the complete basis set limit (CBS) using awCnZ-DK (where n = D, T and Q) using the eqn (1) for the energies.

$$E_n = E_{CBS} + A\exp[-(n-1)] + B\exp[-(n-1)^2] \quad (1)$$

The bond dissociation energy (BDE) of NiO was predicted at the Feller–Peterson–Dixon (FPD) composite thermochemistry level,[56–59] including spin–orbit corrections and the zero-point energies calculated at the icMRCI+Q/awn-DK level.

For the DFT benchmark study, the 43 selected functionals are given in Table 2 and consist of a mix of local spin density approximation (LSDA), general gradient approximations (GGA), meta GGA (mGGA), hybrid GGA (HGGA), and hybrid meta GGA (HmGGA) functionals. The optimization and frequency analysis conducted with the given functionals started with the B3LYP optimized geometry. The DFT calculations were done with the aug-cc-pVDZ basis set on O and the aug-cc-pVDZ-PP basis set on Ni (10 electron pseudopotential on Ni). The DFT calculations were performed at the unrestricted spin level.

A bonding analysis of NiO was performed based on the natural population analysis (NPA) results based on the Natural Bond Orbitals (NBOs)[101,102] using NBO7[103,104] with the MOLPRO program package at the awQ-DK level.

Table 2 DFT exchange–correlation functionals

Method	Exchange	Correlation	Type
B1B95[60]	Becke 96	Becke 95	HmGGA
B1LYP[30,61]	Becke 96	Lee–Yang–Parr	HGGA
B3LYP[27,28]	Becke 93	Lee–Yang–Parr	HGGA
B3P86[28,65]	Becke 93	Perdew 86	HGGA
B3PW91[28]	Becke 93	Perdew–Wang 91	HGGA
B971[64]	Handy–Tozer's modified B97	Handy–Tozer's modified B97	HGGA
B972[65]	Wilson–Bradley–Tozer's modified B97	Wilson–Bradley–Tozer's modified B97	HGGA
B98[66]	Becke 98	Becke 98	HGGA
BP86[62,67]	Becke 88	Perdew 86	GGA
BMK[68]	Boese–Martin	Perdew 86	HGGA
CAM-B3LYP[69]	Becke 88	Lee–Yang–Par	HGGA
HSE06[70–74]	Heyd–Scuseria–Ernzerhof	Perdew–Burke–Ernzerhof	HGGA
HS06[70–74]	Heyd–Scuseria–Ernzerhof	Perdew–Burke–Ernzerhof	HGGA
HSE03[70–74]	Heyd–Scuseria–Ernzerhof	Perdew–Burke–Ernzerhof	HGGA
LC-ωPBE[75]	Perdew–Burke–Ernzerhof	Perdew–Burke–Ernzerhof	HGGA
M052X[76]	Minnesota 05	Minnesota 05	HmGGA
M05[77]	Minnesota 05	Minnesota 05	HmGGA
M062X[78]	Minnesota 062x	Minnesota 062X	HmGGA
M06[78]	Minnesota 06	Minnesota 06	HmGGA
M06HF[79,80]	Minnesota 06HF	Minnesota 06HF	HmGGA
M08HX[81]	Minnesota 08HX	Minnesota 08HX	HmGGA
M11[82]	Minnesota 11	Minnesota 11	HmGGA
MN12SX[83]	Minnesota 12SX	Minnesota 12SX′	HmGGA
MN15[84]	Minnesota 15	Minnesota 15	HmGGA
mPW1LYP[27,85]	Barone's modified PW91	Lee–Yang–Par	HGGA
mPW1PBE[85–87]	Barone's modified PW91	Perdew–Burke–Ernzerhof	HGGA
mPW1PW91[63,85]	Barone's modified PW91	Perdew–Wang 91	HGGA
mPW3PBE[85–87]	Barone's modified PW91	Perdew–Burke–Ernzerhof	HGGA
N12SX[83]	N12SX	N12SX′	HmGGA
O3LYP[27,88]	Handy's OPTX	Lee–Yang–Par	HGGA
PBE1PBE[86,89]	Perdew–Burke–Ernzerhof	Perdew–Burke–Ernzerhof	HGGA
PBEh1PBE[86,90]	98 Revised PBE	Perdew–Burke–Ernzerhof	HGGA
PBE[86]	Perdew–Burke–Ernzerhof	Perdew–Burke–Ernzerhof	GGA
PBE0[89]	Perdew–Burke–Ernzerhof	Perdew–Burke–Ernzerhof	HGGA
PW91[63,91]	Perdew–Wang 1991	Perdew–Burke–Ernzerhof	GGA
SOGGA11X[92]	SOGGA11X	SOGGA11X	HmGGA
SVWN5[93,94]	Slater	VWN Functional V	LSDA
τ-HCTH[95]	τ-Dependent of HCTH	τ-Dependent of HCTH	mGGA
TPSSh[96]	Tao–Perdew–Staroverov–Scuseria	Tao–Perdew–Staroverov–Scuseria	HmGGA
ωB97[97]	Becke 97	Becke 97	HGGA
ωB97X[97]	Becke 97	Becke 97	HGGA
ωB97XD[98,99]	Becke 97	Becke 97	HGGA
X3LYP[27,100]	Becke 97	Becke 97	HGGA

19648 | *Phys. Chem. Chem. Phys.*, 2024, **26**, 19646–19657

This journal is © the Owner Societies 2024

The DFT calculations were done using the Gaussian 16 program.[105] All CCSD(T), CASSCF, CASPT2, and MRCI+Q calculations were performed in the MOLPRO 2021[50–52] computational chemistry program on computers at The University of Alabama, and the Alabama Supercomputing Authority (Dense Memory Cluster).

Results and discussion

Vibrational frequency

In the multiconfiguration and multireference calculations, the two lowest atomic states arising from the $3d^8(^3F)4s^2$ (^3F) and $3d^9(^2D)4s$ (^3D) configurations of Ni were correlated because their associated spin–orbit states are very close in energy. This resulted in a high density of molecular electronic states around the minimum bond distance of the ground state up to 20 000 cm^{-1} relative to the ground state for the SA-CASSCF calculations. A quintet state ($^5\Sigma^-$) was predicted as the ground state, followed by a triplet ($^3\Sigma^-$) state close in energy, with bond distances of about 1.77 Å and 1.69 Å, respectively. Fig. 1 shows this behavior at the SA-CASSCF level.

The inclusion of dynamic correlation effects by icMRCI+Q dramatically changed the description of electronic molecular states of NiO. Spin–orbit effects were also included to check whether possible avoided crossings could change the description of the potential energy curves. However, this did not happen for the Ω states resulting from the ΛS $^5\Sigma^-$ $(\Omega = 0, 1, 2)$ and $^3\Sigma^-$ $(\Omega = 0, 1)$ states. The spin–orbit splitting was 107 cm^{-1} for the ground

Fig. 1 Potential energy curves of the low-lying ΛS singlet, triplet, and quintet SA-CASSCF states.

Table 3 Low-lying states of NiO at the icMRCI+Q/awQ-DK + SO level

State	Ω	ΔE (eV)	ΛS composition
$^3\Sigma_0^-$	0	0.000	98% $^3\Sigma^-$ + 2% $^3\Pi$
$^3\Sigma_1^-$	1	0.006	99% $^3\Sigma^-$ + 1% $^3\Pi$
$^5\Sigma_2^-$	2	0.560	95% $^5\Sigma^-$ + 4% $^3\Pi$
$^5\Sigma_1^-$	1	0.560	99% $^5\Sigma^-$ + 1% $^3\Pi$
$^5\Sigma_0^-$	0	0.560	100% $^5\Sigma^-$

state $^3\Sigma^-$ $(\Omega = 0)$ and the first excited state $^3\Sigma^-$ $(\Omega = 1)$. Table 3 presents the composition of the spin–orbit states that correlate to the $^5\Sigma^-$ and $^3\Sigma^-$ states. Fig. 2 shows the spin–orbit icMRCI+Q/awQ-DK potential energy curves up to 8000 cm^{-1}. The ground state at the icMRCI+Q level was predicted to be the $^3\Sigma_0^-$ and lies more than 4000 cm^{-1} below the $^5\Sigma_2^-$ state; thus, there is no crossing between the triplet and quintet states as was found at the SA-CASSCF level. There is no significant change in the shape of the PECs and the energy splitting due to the spin–orbit effects is small for NiO, so the following analysis will focus on the ΛS states. Table 4 presents the spectroscopic parameters calculated for the ground state ($^3\Sigma^-$) of NiO using the awT-DK and awQ-DK basis sets, and the extrapolation to the complete basis set (CBS) limit. The basis set has very little effect on the bond distance, which shows a small shortening as more functions are included in the basis set, as well as a small decrease in the ω_e and $\omega_e x_e$. The inclusion of spin–orbit coupling lowers the energy of the ground state by 111 cm^{-1} relative to the value without spin orbit and has no significant impact on the bond distance. In the spin–orbit calculation, a small change in the shape of the PECs around the bond distance decreases the ω_e and $\omega_e x_e$ for the Ω states associated with the ΛS $^3\Sigma^-$ state.

Coupled cluster theory at the CCSD(T) level was used as the benchmark of the single reference methods as shown in Table 4. There is a modest basis set effect from aD to aT with the overall bond distance decreasing by 0.01 Å, and the ω_e increasing by 20 cm^{-1}. However, there is little effect of increasing the basis set from aT to aQ on the bond distance and frequency. When correlating the outer core electrons in the system, the bond distance is very similar to the calculations correlating only the valence electrons. The effect on the ω_e is modest with the frequencies being roughly 10 cm^{-1} less than valence only calculations. There are large T_1 values for the CCSD(T) calculations showing substantial multi-reference character which arises from the $3d^8(^3F)4s^2$ (^3F) and $3d^9(^2D)4s$ (^3D) configurations as described above. The quintet state is 149 kJ mol^{-1} above the triplet at the awcTZ-DK level of theory.

The potential energy curve calculated at the CCSD(T)/awCQ-DK level is given in Fig. 3. Potential energy curves calculated at the CCSD(T) level were obtained at intervals of 0.01 Å as the frequency of NiO is highly sensitive to R_e, and to appropriately model the $^5\Sigma^-$ $(\Omega = 0, 1, 2)$ and $^3\Sigma^-$ $(\Omega = 0)$ state crossing that occurs at approximately at 1.62 Å in the multi-reference calculations. When compared to the results from the multireference and multiconfigurational calculations, icMRCI+Q and CASSCF, respectively, CCSD(T) consistently overestimates ω_e. Fig. 3 shows an overlay the potential energy curves from the
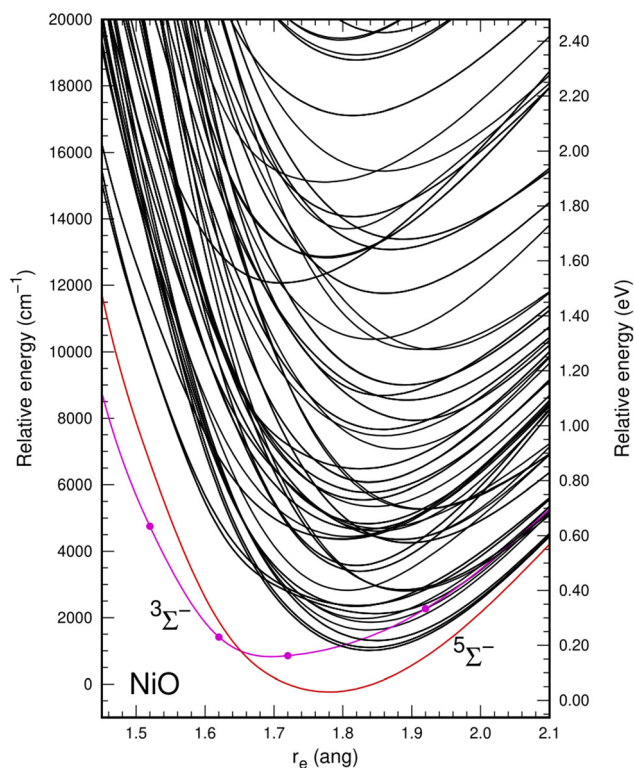
This journal is © the Owner Societies 2024

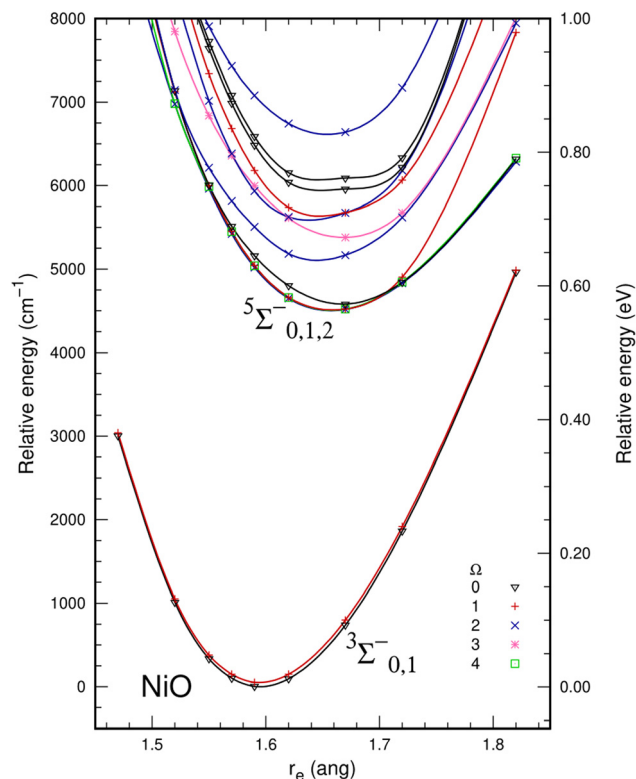*Phys. Chem. Chem. Phys.*, 2024, **26**, 19646–19657 | **19649**

Fig. 2 Potential energy curves of the low-lying Ω states using the spin–orbit icMRCI+Q energies.

Table 4 Spectroscopic parameters for the ground state ($^3\Sigma^-$) of NiO calculated at the icMRCI+Q/awn-DK (n = T, Q) level

Method	Basis set	r_e/Å	ω_e/cm^{-1}	$\omega_e x_e$	T_1
icMRCI+Q	awT-DK	1.6023	838.5	^{a}	
icMRCI+Q	awQ-DK	1.6003	836.1	^{a}	
icMRCI+Q	CBS	1.5992	835.0	^{a}	
CCSD(T)	aD-DK	1.63628	865.6	1.87	0.129
CCSD(T)	aT-DK	1.62481	889.08	2.08	0.126
CCSD(T)	aQ-DK	1.62276	889.40	1.93	0.126
CCSD(T)	CBS	1.62177	888.80	1.82	
CCSD(T)	awT-DK	1.62496	876.09	2.29	0.1029
CCSD(T)	awQ-DK	1.62425	873.54	1.94	0.1029
CCSD(T)	CBS	1.62384	872.07	1.74	

^{a} $\omega_e x_e$ was not calculated. See Computational section for discussion.

CCSD(T), MRCI, MRCI+Q, and CASSCF calculations. Therefore, as a benchmark, methods other than CCSD(T) should be used due to the highly multireference character of the Ni–O bond.

Thermochemistry

The bond dissociation energies (BDEs) of NiO calculated at CCSD(T)/awn-DK and icMRCI+Q/awn-DK levels are given in Table 5. Spin–orbit (SO) constants were calculated at the icMRCI+Q/awn-DK level and these numbers were used to estimate the final BDE values in both cases. Due to the excessive number of singlet, triplet, and quintet electronic molecular states correlating to the two lowest dissociation
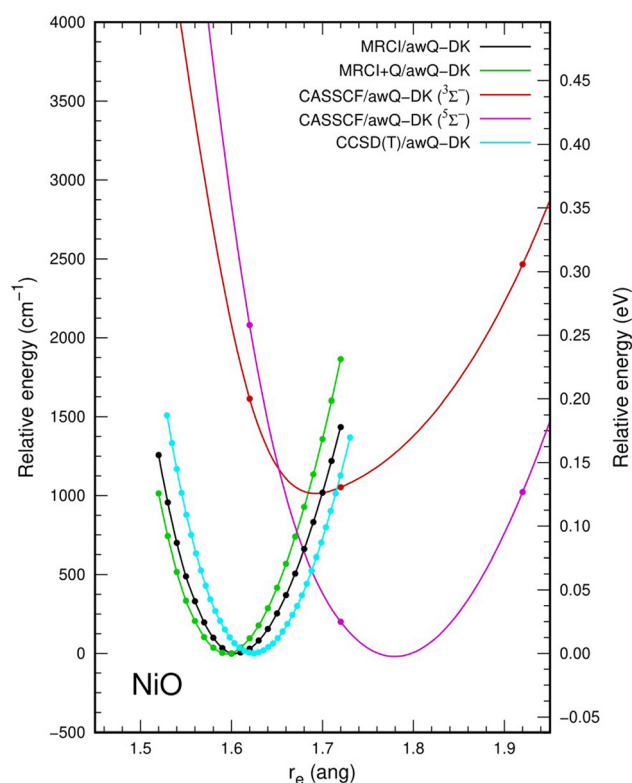

Fig. 3 Potential energy curves of the ground $^3\Sigma^-$ state calculated at the CCSD(T)/awQ-DK level (light blue), the potential energy curve of the $^3\Sigma^-$ state calculated at the icMRCI/awQ-DK level (black), the potential energy curve of the $^3\Sigma^-$ state calculated at the icMRCI+Q/awQ-DK level (green), the potential energy curve of the $^5\Sigma^-$ state calculated at the CASSCF/awQ-DK level (red), and the potential energy curve of the $^3\Sigma^-$ state calculated at the CASSCF/awQ-DK level (purple).

channels, Ni(^3F_g) + O(^3P_g) and Ni(^3D_g) + O(^3P_g), the icMRCI+Q did not converge properly at the dissociation limit. Therefore, only the NiO triplet states (9 A_1, 9 B_1, 9 B_2, 9 A_2) were optimized in the SA-CASSCF, and these states were taken as a reference for the ground state optimization in the icMRCI+Q. The L_z^2 numbers confirmed the correct convergence in the asymptotic limit at r(Ni–O) = 6 Å.

For the CCSD(T) calculations, the BDE was calculated relative to separate atomic energies, instead of using the supermolecule approximation used for icMRCI+Q. Due to the multi-reference nature of the triplet ground state, the BDE at the FPD/CCSD(T) level was first calculated relative to the excited quintet state where the T_1 values are much smaller showing less multi-reference character. The BDE of the ground triplet state was then obtained by using the icMRCI+Q adiabatic energy difference between the triplet ground state and the excited quintet state.

We have previously found that the CCSD(T) energies can be improved by using orbitals from density functional theory.[106–108] Thus, another approach to the prediction of the BDE of NiO is to use orbitals generated at the DFT level using the PW91 functional for the triplet state. This approach led to reasonable values of the T_1 diagnostic[109] on the order of 0.015. The BDE for the triplet state was substantially improved over

19650 | *Phys. Chem. Chem. Phys.*, 2024, **26**, 19646–19657

This journal is © the Owner Societies 2024

Table 5 BDE (kJ mol^{-1}) including the spin–orbit and zero-point energy (ZPE) corrections calculated at the CCSD(T)/awn-DK and icMRCI+Q/awn-DK levels

Calculation	awT-DK	awQ-DK	CBS (awn-DK)
CCSD(T) Quintet	238.0	235.6	234.2
icMRCI+Q	388.8	398.7	404.3
SO constant (Ni)	12.0	12.0	12.0
SO constant (O)	0.9	1.0	1.0
SO constant (NiO $^3\Sigma^-$)	1.3	1.3	1.3
SO constant (NiO $^5\Sigma^-$)	7.2	3.3	1.0
ZPE correction $^3\Sigma^-$	5.0	5.0	5.0
ZPE correction $^5\Sigma^-$	3.2	3.3	3.3
FPD/CCSD(T) $^5\Sigma^-$	229.1	222.6	218.9
FPD/CCSD(T) $^3\Sigma^-$	362.6	356.1	352.4
Final icMRCI+Q $^3\Sigma^-$	372.2	382.1	387.7
Watson et al.[16]			373.2
Farber and Srivastava[20]			349.4 ± 6.3

that using the HF orbitals for the CCSD calculations and is within 10 kJ mol^{-1} of the value from the quintet state.

The calculated FPD/CCSD(T) and icMRCI+Q BDEs of the triplet ground state of NiO are not in particularly good agreement with each other, differing by 37 kJ mol^{-1}. The experimental results Farber and Srivastava[20] and Watson et al.[16] differ by 24 kJ mol^{-1} so they cannot be used to help in distinguishing between the two calculated values. The FPD value is consistent with the lower value of 349.4 ± 6.3 kJ mol^{-1} [20] within the error bars. The icMRCI+Q value is 14 kJ mol^{-1} greater than the larger experimental value of 372.2 kJ mol^{-1}.[16]

Electronic structure

The orbital populations and the charges (q) from NBO analysis for NiO are shown in Table 6. The NBO analysis in Table 7 shows that NiO has significant ionic interactions with a highly polarized σ bond that is predominantly composed of the $2p_z$ on O and the 4s on Ni. Two α unpaired electrons associated with the dπ non-bonding orbitals on nickel result in the $^3\Sigma^-$ ground state. Fig. 4 also shows the SA-CASSCF natural orbitals at the awQ-DK level associated with the nine electrons correlated in the 14 orbitals of the active space. The icMRCI+Q wavefunction for the ground state indicates a strong multireference character. The corresponding major contributions are given in eqn (2)

$$0.71\,|1\sigma^2 1\delta^4 2\sigma^2 1\pi^4 2\pi^2\rangle - 0.39\,|1\sigma^2 1\delta^4 2\sigma^1 3\sigma^1 1\pi^4 2\pi^2\rangle \tag{2}$$

There are 10 additional configurations whose coefficients range from 0.10 to 0.20. The triplet state is comprised of two α unpaired electrons associated with the dπ non-bonding orbitals on Ni. Further NBO analysis shows that NiO has significant

Table 6 NPA charges (q) and population for NiO at awQ-DK level

Property	NiO ($^3\Sigma^-$)
q(Ni)	1.405
q(O)	−1.405
4s (4sα/4sβ)	0.49 (0.24/0.24)
3d (3dα/3dβ)	8.07 (4.96/3.11)
O 2p (2pα/2pβ)	5.39 (2.76/2.63)

Table 7 NBOs of NiO at the awQ-DK level

NBO	Symmetry	occ	Ni%q	Ni%s	Ni%d	O%q	O%s	O%p
Ni–O	σ	2.000	23.7	96.3	3.3	76.3	6.1	93.6
LP(Ni)	δ	4.000	100	0.0	100			
LP(Ni)	σ	1.998	100	3.2	96.8			
LP(Ni) α	π	1.994	100	0.0	99.9			
LP(O)	σ	1.998				100	94.1	5.9
LP(O)	π	3.982				100	0.0	100
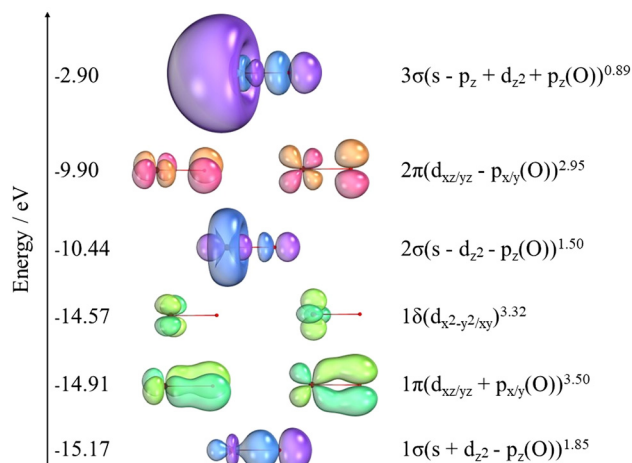
Fig. 4 Natural orbitals (SA-CASSCF/awQ-DK) energies and composition for the 14 electrons correlated in the active space. Unlabeled orbitals are on Ni. Ni on the left and O on the right. 80% of the surfaces were accounted for.

ionic interactions and a σ bond that is mostly a p_z of oxygen combined with the 4s of nickel.

Benchmarking DFT functionals: frequency

Table 8 shows ω_e and r_e calculated using 43 DFT functionals benchmarked against the best multireference value and experiment. Of the functionals tested, 3 functionals predicted ω_e in reasonable agreement with experiment and the icMRCI+Q calculations. The three best functionals were CAM-B3LYP, τ-HCTH, and ωB97xd, which predicted ω_e within 5 cm^{-1} of experiment and of the icMRCI+Q calculations. CAM-B3LYP is a long-range corrected form of B3LYP utilizing the Coulomb-attenuating method (CAM). CAM-B3LYP overestimates the Ni–O bond length by approximately 0.02 Å from the experimental value[12] of 1.62712 Å and 0.04 Å from the icMRCI+Q value. The CAM-B3LYP result differs from experiment[13] by 7.3 cm^{-1} and from icMRCI+Q calculations by 3.3 cm^{-1}. The ωB97XD functional which also includes long range interactions differs from experiment by 0.8 cm^{-1} and by 3.2 cm^{-1} from the best calculated value. The τ-HCTH meta GGA functional differs by 1.7 cm^{-1} from experiment and 2.4 cm^{-1} from icMRCI+Q. In comparison to the best functionals, commonly used functionals such as B3LYP, PBE, and M06 predict ω_e values that are not in agreement with experiment. The B3LYP value is ∼ 50 cm^{-1} larger than experiment and similar to the CCSD(T)

This journal is © the Owner Societies 2024

Phys. Chem. Chem. Phys., 2024, **26**, 19646–19657 | **19651**

Table 8 Spectroscopic parameters for the ground state ($^3\Sigma^-$) of NiO calculated at the DFT/aD level

Functional	r_e (Å)	ω_e (cm^{-1})	ΔExpt (cm^{-1})	ΔicMRCI+Q (cm^{-1})
B1B95	1.605	900.8	61.7	65.8
B1LYP	1.612	892.2	53.1	57.2
B3LYP	1.611	888.5	49.4	53.5
B3P86	1.601	908.8	69.7	73.8
B3PW91	1.605	901.5	62.4	66.5
B971	1.651	743.1	96.0	91.9
B972	1.608	884.4	45.3	49.4
B98	1.650	743.1	96.0	91.9
BP86	1.616	866.6	27.5	31.6
BMK	1.603	945.6	106.5	110.6
CAM-B3LYP	1.647	838.3	0.8	3.3
HSE06	1.602	910.4	71.3	75.4
HS06	1.602	910.2	71.1	75.2
HSE03	1.603	911.3	72.2	76.3
LC-ωPBE	1.590	959.2	120.1	124.2
M052X	1.621	911.3	72.2	76.3
M05	1.623	887.0	47.9	52.0
M062X	1.625	875.6	36.5	40.6
M06	1.599	913.4	74.3	78.4
M06HF	1.673	797.2	41.9	37.8
M08HX	1.632	884.0	44.9	49.0
M11	1.618	919.8	80.7	84.8
MN12SX	1.595	938.3	99.2	103.3
MN15	1.624	873.8	34.7	38.8
mPW1LYP	1.611	893.2	54.1	58.2
mPW1PBE	1.605	911.9	72.8	76.9
mPW1PW91	1.602	910.5	71.4	75.5
mPW3PBE	1.603	903.9	64.8	68.9
N12SX	1.645	801.9	37.2	33.1
O3LYP	1.616	858.9	19.8	23.9
PBE1PBE	1.602	910.0	70.9	75.0
PBEh1PBE	1.602	912.0	72.9	77.0
PBE	1.617	862.4	23.3	27.4
PPE0	1.600	917.0	77.9	82.0
PW91	1.617	866.4	27.3	31.4
SOGGA11X	1.663	758.4	80.7	76.6
SVWN5	1.586	925.9	86.8	90.9
τ-HCTH	1.621	837.4	1.7	2.4
TPSSh	1.611	889.3	50.2	54.3
ωB97	1.596	947.6	108.5	112.6
ωB97X	1.644	853.9	14.8	18.9
ωB97XD	1.652	831.8	7.3	3.2
X3LYP	1.610	892.0	52.9	57.0

values. Furthermore, PBE and M06 are 70 cm^{-1} and 80 cm^{-1} larger than experiment, respectively.

Benchmarking DFT functionals: Ni–O BDE

The Ni–O BDEs with different functionals are given in Table 9. We derive BDE(1) and BDE(2) from eqn (3) and (4) respectively,

$$NiO \rightarrow {}^3Ni + {}^3O \qquad (3)$$

$$NiO \rightarrow {}^1Ni + {}^3O \qquad (4)$$

For BDE(1) (eqn (3)), the correction to the ground triplet state of the Ni is taken from experiment[110,111] based on the electronic configuration found by the NBO analysis of the atom. The ground state of Ni is ^{3}F (3d^{8}4s^2) with the ^{3}D (3d^{9}4s^1) excited state 204.787 cm^{-1} higher in energy. BDE(2) (eqn (4)) arising from singlet Ni can be corrected to the ground state Ni using a similar approach. There are two open shell singlet ^{1}D states corresponding to the 3d^9 s^1 configuration at 3409.937 cm^{-1} and

the 3d^{8}4s^2 configuration at 13 521.347 cm^{-1}. The closed shell ^{1}S state corresponding to the 3d^{10} configuration is at 14 728.840 cm^{-1}.

In contrast to the issues with the frequency calculations, 16 DFT functionals predicted BDE(1) value within 20 kJ mol^{-1} of the FPD BDE, with 4 functionals, HS06, HSE03, MN15, and PBE1PBE, predicting the BDE within 4 kJ mol^{-1} of the FPD value. A majority of the functionals predicted the ^{3}D excited state of Ni as the ground state instead of the ^{3}F state, although this corresponds to only a small energy correction of 2.5 kJ mol^{-1}. The top three performing functionals for the frequency calculations, CAM-B3LYP, τ-HCTH, and ωB97XD all performed poorly, with ΔBDE(1) values of 138.2, −125.2, and 113.7 kJ mol^{-1}, respectively. Calculating the Ni–O BDE with respect to a singlet Ni and correcting the energy with the singlet–triplet splitting of Ni giving BDE(2) does improve many of the poorly performing functionals including CAM-B3LYP and τ-HCTH. The PBE0 functional is in essentially exact agreement with the FPD value. A limitation on the BDE(2) values is the state of the Ni as taken from the NBO analysis as most of the atomic singlet Ni DFT calculations go to an open shell s^{1}d^9 singlet rather than the closed shell d^{10} configuration which introduces additional errors.

Conclusions

The vibrational frequency, bond dissociation energy, and electronic structure of NiO were calculated using a range of methodologies including CASSCF, icMRCI+Q, CCSD(T), and DFT. CASSCF predicted a quintet state ($^5\Sigma^-$) ground state for the equilibrium bond distance with a state crossing occurs at 1.65 Å, where the triplet ($^3\Sigma^-$) state becomes lower energy. icMRCI+Q predicts a triplet ($^3\Sigma^-$) state as the ground state and does not predict a state crossing. The ground state results from the ionic interaction of the O 2p$_z$ bonding with the 4s/3d$_{z^2}$ of Ni to form a σ bond. The inclusion of dynamic correlation effects at the icMRCI+Q level altered the electronic structure predicted by CASSCF. At the icMRCI+Q level, the ground state is $^3\Sigma^-$ in agreement with experiment.[12,13] The frequency calculated at the icMRCI+Q/CBS level is within 4.1 cm^{-1} of experiment,[13] and the bond distance is within 0.028 Å of experiment.[12] The calculated values show little effect of increasing basis set size, with frequencies deviating from the complete basis set level by 3 cm^{-1} for the triple zeta basis set, and 1 cm^{-1} for the quadruple basis set.

To benchmark the accuracy of non-multireference methods for the frequency, CCSD(T) and DFT were used. CCSD(T) predicts vibrational frequencies that are ∼ 50 cm^{-1} too high due to the multireference character of the ground triplet state. Correlation of the outer core electrons of Ni improves the calculated frequency but the value still differs by ∼40 cm^{-1} from experiment. An array of 43 DFT functionals waas benchmarked. The 3 best functionals out of the 43 tested are ωB97XD, CAM-B3LYP, and τ-HCTH which gave frequencies within <10 cm^{-1} of experiment.

The BDE of NiO was calculated at the FPD/CCSD(T) and icMRCI+Q levels as well as with the 43 DFT functionals. The

19652 | *Phys. Chem. Chem. Phys.*, 2024, **26**, 19646–19657

This journal is © the Owner Societies 2024

Table 9 Bond dissociation energies (BDE) in kJ mol^{-1} for NiO calculated at the DFT/aD level with different functionals

Functional	BDE(1)	ΔBDE(1)	Ni config BDE(1)[a]	BDE(2)	ΔBDE(2)	Ni config BDE(2)[a]
B1B95	347.5	4.9	[Ar]s^{1}d^9	372.4	−20.0	[Ar]d^{10}
B1LYP	334.9	17.5	[Ar]s^{1}d^9	455.6	−103.2	[Ar]s^{1}d^9
B3LYP	367.0	−14.6	[Ar]s^{1}d^9	475.1	−122.7	[Ar]s^{1}d^9
B3P86	383.7	−31.3	[Ar]s^{1}d^9	551.1	−198.7	[Ar]s^{1}d^9
B3PW91	363.3	−10.9	[Ar]s^{1}d^9	500.5	−148.1	[Ar]d^{10}
B971	309.7	42.7	[Ar]s^{2}d^8	457.0	−104.6	[Ar]s^{1}d^9
B972	379.3	−26.9	[Ar]s^{1}d^9	466.2	−113.8	[Ar]s^{1}d^9
B98	304.0	48.4	[Ar]s^{1}d^9	376.9	−24.5	[Ar]d^{10}
BP86	463.0	−110.6	[Ar]s^{1}d^9	545.1	−192.7	[Ar]s^{1}d^9
BMK	389.5	−37.1	[Ar]s^{2}d^8	565.9	−213.5	[Ar]d^{10}
CAM-B3LYP	214.2	138.2	[Ar]s^{1}d^9	380.2	−27.8	[Ar]s^{1}d^9
HSE06	191.3	161.1	[Ar]s^{1}d^9	323.7	28.7	[Ar]s^{1}d^9
HS06	348.5	3.9	[Ar]s^{1}d^9	480.0	−128.5	[Ar]s^{1}d^9
HSE03	349.8	2.6	[Ar]s^{1}d^9	482.6	−130.2	[Ar]s^{1}d^9
LC-ωPBE	368.2	−15.8	[Ar]s^{1}d^9	507.2	−154.8	[Ar]s^{1}d^9
M052X	307.2	45.2	[Ar]s^{1}d^9	337.6	14.8	[Ar]d^{10}
M05	374.0	−21.6	[Ar]s^{1}d^9	328.0	24.4	[Ar]d^{10}
M062X	262.4	90.0	[Ar]s^{1}d^9	294.0	58.4	[Ar]d^{10}
M06	364.6	−12.2	[Ar]s^{1}d^9	451.5	−99.1	[Ar]s^{1}d^9
M06HF	189.5	162.9	[Ar]s^{1}d^9	307.4	45.0	[Ar]d^{10}
M08HX	291.6	60.8	[Ar]s^{1}d^9	459.5	−107.1	[Ar]d^{10}
M11	326.1	26.3	[Ar]s^{2}d^8	438.8	−86.4	[Ar]s^{1}d^9
MN12SX	251.9	100.5	[Ar]s^{2}d^8	384.9	−32.5	[Ar]s^{2}d^8
MN15	353.7	−1.3	[Ar]s^{1}d^9	288.5	63.9	[Ar]d^{10}
mPW1LYP	342.7	9.7	[Ar]s^{1}d^9	461.3	−108.9	[Ar]s^{1}d^9
mPW1PBE	342.3	10.1	[Ar]s^{1}d^9	393.8	−41.4	[Ar]d^{10}
mPW1PW91	338.7	13.7	[Ar]s^{1}d^9	390.3	−37.9	[Ar]d^{10}
mPW3PBE	371.5	−19.1	[Ar]s^{1}d^9	489.6	−137.2	[Ar]s^{1}d^9
N12SX	264.4	88.0	[Ar]s^{2}d^8	444.7	−92.3	[Ar]s^{1}d^9
O3LYP	385.3	−32.9	[Ar]s^{1}d^9	466.7	−114.3	[Ar]s^{1}d^9
PBE1PBE	349.4	3.0	[Ar]s^{1}d^9	479.8	−127.4	[Ar]s^{1}d^9
PBEh1PBE	347.8	4.6	[Ar]s^{1}d^9	479.9	−127.5	[Ar]s^{1}d^9
PBE	469.5	−117.1	[Ar]s^{1}d^9	546.7	−194.3	[Ar]s^{1}d^9
PPE0	245.9	106.5	[Ar]s^{1}d^9	352.2	0.2	[Ar]d^{10}
PW91	469.8	−117.4	[Ar]s^{1}d^9	549.4	−197.0	[Ar]s^{1}d^9
SOGGA11X	464.6	−112.2	[Ar]s^{1}d^9	512.8	−160.4	[Ar]d^{10}
SVWN5	587.6	−235.2	[Ar]s^{1}d^9	636.1	−283.7	[Ar]s^{1}d^9
τ-HCTH	477.6	−125.2	[Ar]s^{1}d^9	358.9	−6.5	[Ar]s^{2}d^8
TPSSh	396.0	−43.6	[Ar]s^{1}d^9	499.3	−146.9	[Ar]s^{1}d^9
ωB97	374.5	−22.1	[Ar]s^{1}d^9	620.5	−268.1	[Ar]s^{1}d^9
ωB97X	240.4	112.0	[Ar]s^{1}d^9	358.6	−6.2	[Ar]d^{10}
ωB97XD	238.7	113.7	[Ar]s^{1}d^9	283.7	68.7	[Ar]d^{10}
X3LYP	362.4	−10.0	[Ar]s^{1}d^9	473.9	−121.5	[Ar]s^{1}d^9

[a] Ni atom configuration from the NBO analysis.

available experimental data[16,20] are not in good enough agreement to distinguish between the FPD/CCSD(T) and icMRCI+Q BDE values for the NiO BDE. The FPD/CCSD(T) value of 352 kJ mol^{-1} is consistent with the experimental[20] BDE of 349.4 ± 6.3 kJ mol^{-1} whereas the icMRCI+Q BDE of 388 kJ mol^{-1} is larger than the largest experimental[16] value by 14 kJ mol^{-1}. The results show that further experimental investigation of the thermodynamics of the NiO bond is needed. The DFT values for 16 functionals are in agreement within 20 kJ mol^{-1} of the FPD/CCSD(T) value using the BDE(1) expression but these do not include the 3 best functionals for the frequency predictions. The 3 best frequency functionals have errors ranging from −125 to 138 kJ mol^{-1} using the BDE(1) expression. Use of the state splitting corrected BDE(2) expression substantially improved the BDE values for the CAM-B3LYP and τ-HCTH functionals, especially the latter value. Note that the use of the BDE(2) expression resulted in worse agreement for most functionals. It is important to calculate the electronic state of the Ni atom used in the BDE equation with

each functional so an appropriate experimental correction for the excited state-ground state splitting can be applied.

Comparison of the multireference and single reference results shows that the MRCI approach gives a bond distance for the $^3\Sigma^-$ ground state that is a bit too short but has the right curvature; in contrast, the single reference based CCSD(T) method with a large T_1 value demonstrating multireference character yields a good bond distance, but the predicted curvature is too tight. The CCSD(T) method predicts a good bond energy if the energy of the excited $^5\Sigma^-$ state which is dominated by a single configuration. The BDE for the ground $^3\Sigma^-$ state can then be obtained by the energy difference between the $^3\Sigma^-$ and $^5\Sigma^-$ states. The MRCI approach predicts a BDE that is likely to be too large and this can be attributed to the difficulty in calculating the energy at large R. Selected DFT functionals can predict the bond distance and vibrational frequency with some reliability but fail in predicting the BDE unless a carefully selected set of atomic states is chosen.

The current work demonstrates that the vibrational frequency and BDE of NiO can be reliably calculated using advanced correlated molecular orbital theory approaches. If one starts with a single reference-based method such as CCSD(T), the T_1 values should be carefully checked for the presence of multi-reference character. When using DFT, it is important to be careful about the choice of the functional as commonly used functionals such as PBE and B3LYP perform poorly when calculating both the spectroscopic properties and BDE of NiO. In addition, care must be taken to examine the electronic state of the bare metal atom as it may not be the ground state. For more complex NiO based systems, it will be important to carefully choose the functional and compromise may need to be made for getting the best functional in terms of vibrational spectroscopy predictions and reaction energies.

Data availability

The data supporting this article have been included as part of the Supplementary Information.

Conflicts of interest

There are no conflicts to declare.

Acknowledgements

References

1 Y. Lingting and K. Xie, High-Temperature Electrocatalysis and Key Materials in Solid Oxide Electrolysis Cells, *J. Eng. Chem*, 2021, **54**, 736–745.

2 C. Graves, S. D. Ebbesen and M. Mogensen, Co-Electrolysis of CO_2 and H_2O in Solid Oxide Cells: Performance and Durability, *Solid State Ionics*, 2011, **192**, 398–403.

3 Y. Tao, S. D. Ebbesen and M. B. Mogensen, Carbon Deposition in Solid Oxide Cells during Co-Electrolysis of H_2O and CO_2, *J. Electrochem. Soc.*, 2014, **161**, F337–F343.

4 S. D. Ebbesen, X. Sun and M. B. Mogensen, Understanding the Processes Governing Performance and Durability of Solid Oxide Electrolysis Cells, *Faraday Disc.*, 2015, **182**, 393–422.

5 S. D. Ebbesen, C. Graves and M. Mogensen, Production of Synthetic Fuels by Co-Electrolysis of Steam and Carbon Dioxide, *Int. J. Green Energy*, 2009, **6**, 646–660.

6 Y. Zheng, J. Wang, B. Yu, W. Zhang, J. Chen, J. Qiao and J. Zhang, A Review of High Temperature Co-Electrolysis of H_2O and CO_2 to Produce Sustainable Fuels Using Solid Oxide Electrolysis Cells (SOECs): Advanced Materials and Technology, *Chem. Soc. Rev.*, 2017, **46**, 1427–1463.

7 Y. Li, P. Li, B. Hu, C. Xia and A. Nanostructured, Ceramic Fuel Electrode for Efficient CO_2/H_2O Electrolysis Without Safe Gas, *J. Mat. Chem. A*, 2016, **4**, 9236–9243.

8 S. Ebbesen, R. Knibbe and M. Mogensen, Co-Electrolysis of Steam and Carbon Dioxide in Solid Oxide Cells, *J. Electrochem. Soc.*, 2012, **159**, F482–F489.

9 J. Carneiro and E. Nikolla, Nanoengineering of Solid Oxide Electrochemical Cell Technologies: An Outlook. *Nano, Research*, 2019, **12**, 2081–2092.

10 M. Laguna-Bercero, Recent Advances in High Temperature Electrolysis Using Solid Oxide Fuel Cells: A Review, *J. Power Sources*, 2012, **203**, 4–16.

11 X.-K. Gu and E. Nikolla, Fundamental Insights into High-Temperature Water Electrolysis Using Ni-Based Electrocatalysts, *J. Phys. Chem. C*, 2015, **119**, 26980–26988.

12 R. S. Ram and P. F. Bernath, Fourier Transform Infrared Emission Spectroscopy of a New A $^3\Pi_i$–X $^3\Sigma^-$ System of NiO, *J. Mol. Spectrosc.*, 1992, **155**, 315–325.

13 V. I. Srdanov and D. O. Harris, Laser Spectroscopy of NiO: The $^3\Sigma^-$ Ground State, *J. Chem. Phys*, 1988, **89**, 2748–2753.

14 D. W. Green, G. T. Reedy and J. G. Kay, Matrix Isolated FeO. NiO, and CoO: Ground State Vibratioonal Frequencies, *J. Mol. Spectrscop.*, 1979, **78**, 257–266.

15 Hongbin Wu and L.-S. Wang, A Study of Nickel Monoxide (NiO), Nickel Dioxide (OniO), and Ni(O$_2$) Complex by Anion Photoelectron Spectroscopy, *J. Chem. Phys.*, 1997, **107**, 16–21.

16 L. R. Watson, T. L. Thiem, R. A. Dressler, R. H. Salter and E. Murad, High Temperature Mass Spectrometric Studies of the Bond Energies of Gas-Phase ZnO, NiO, and CuO, *J. Phys. Chem.*, 1993, **97**, 5577–5580.

17 K. Namiki and S. Saito, Microwave Spectrum of the NiO Radical in the X $^3\Sigma^-$ State, *Chem. Phys. Lett.*, 1996, **252**, 343–347.

18 T. M. Ramond, G. E. Davico, F. Hellberg, F. Svedberg, P. Salén, P. Söderqvist and W. C. Lineberger, Photoelectron Spectroscopy of Nickel, Palladium, and Platinum Oxide Anions, *J. Mol. Spectrosc.*, 2002, **216**, 1–14.

19 D. A. Burgard, J. Abraham, A. Allen, J. Craft, W. Foley, J. Robinson, B. Wells, C. Xu and D. H. Stedman, Chemiluminescent Reactions of Nickel, Iron, and Cobalt Carbonyls with Ozone, *Appl. Spectrosc.*, 2006, **60**, 99–102.

20 M. Farber and R. D. Srivastava, The Dissociation Energy of NiO and Vaporization Sublimation Enthalpies of Ni, *Anal. Calorimetry*, 1974, **3**, 731–741.

21 E. R. Fisher and P. B. Armentrout, Reactions of Co$^+$, Ni$^+$, and Cu$^+$ with Cyclopropane and Ethylene Oxide. Metal-Methylidene Ion Bond Energies, *J. Phys. Chem.*, 1990, **94**, 1674–1683.

22 S. P. Walch and W. A. Goddard III, Electronic States of the Nickel Oxide Molecule, *J. Am. Chem. Soc.*, 1978, **100**, 1338–1348.

23 M. Dolg, W. H. Stoll and H. Preuss, *Ab initio* Pseudopotential Study of the First Row Transition Metal Monoxides and Iron Monohydride, *J. Chem. Phys*, 1987, **86**, 2123–2131.

19654 | *Phys. Chem. Chem. Phys.*, 2024, **26**, 19646–19657

This journal is © the Owner Societies 2024

24 C. W. Bauschlicher, C. J. Nelin and P. S. Bagus, Transition Metal Oxides: CrO, MoO, NiO, PdO, AgO, *J. Chem. Phys*, 1985, **82**, 3265–3276.

25 M. A. Abdulsattar and M. T. Matrood, Spin Multiplicity Effects on Electronic and Spectroscopic Properties of NiO Diatomic Molecule: A DFT Study, *AIP Conf. Proc.*, 2023, **2845**, 070029.

26 C. W. Bauschlicher and P. Maitre, Theoretical Study of First Transition Row Oxides and Sulfides, *Theor. Chim. Acta*, 1995, **90**, 189–203.

27 C. Lee, W. Yang and R. G. Parr, Development of the Colle-Salvetti Correlation-Energy Formula into a Functional of the Electron Density, *Phys. Rev. B*, 1988, **37**, 785–789.

28 A. D. Becke, Density-Functional Thermochemistry. III. The Role of Exact Exchange, *J. Chem. Phys.*, 1993, **98**, 5648–5652.

29 W. Kohn, A. D. Becke and R. G. Parr, Density Functional Theory of Electronic Structure, *J. Phys. Chem.*, 1996, **100**, 12974–12980.

30 T. H. Dunning, Gaussian Basis Set for Use in Correlated Molecular Calculations. I. The Atoms Boron Through Neon and Hydrogen, *J. Chem. Phys.*, 1989, **90**, 1007–1023.

31 R. A. Kendall, T. H. Dunning, Jr. and R. J. Harrison, Electron Affinities of the First-Row Atoms Revisited. Systematic Basis Sets and Wave Functions, *J. Chem. Phys.*, 1992, **96**, 6796–6806.

32 M. Dolg, Improved Relativistic Energy-Consistent Pseudopotentials for 3d-Transition Metals, *Theor. Chem. Acc.*, 2005, **114**, 297–304.

33 S. Li, J. M. Hennigan, D. A. Dixon and K. A. Peterson, Accurate Thermochemistry for Transition Metal Oxide Clusters, *J. Phys. Chem. A*, 2009, **113**, 7861–7877.

34 The basis sets for Ni are available from Prof. Kirk Peterson, Washington State University. **https:1/chem.wsu.edu/people/faculty/wsu-profile/kipeters/** (Accessed September 1, 2023).

35 G. D. Purvis and R. J. Bartlett, A Full Coupled-Cluster Singles and Doubles Model: The Inclusion of Disconnected Triples, *J. Chem. Phys.*, 1982, **76**, 1910–1918.

36 K. Raghavachari, G. W. Trucks, J. A. Pople and M. Head-Gordon, A Fifth-order Perturbation Comparison of Electron Correlation Theories, *Chem. Phys. Lett.*, 1989, **157**, 479–483.

37 J. D. Watts, J. Gauss and R. J. Bartlett, Coupled-Cluster Methods with Non-iterative Triple Excitations for Restricted Open-Shell Hartree–Fock and Other General Single-Determinant Reference Functions. Energies and Analytical Gradients, *J. Chem. Phys.*, 1993, **98**, 8718–8733.

38 R. J. Bartlett and M. Musial, Coupled-Cluster Theory in Quantum Chemistry, *Rev. Mod. Phys.*, 2007, **79**, 291–352.

39 M. J. O. Deegan and P. J. Knowles, Perturbative Corrections to Account for Triple Excitations in Closed and Open Shell Coupled Cluster Theories, *Chem. Phys. Lett.*, 1994, **227**, 321–326.

40 M. Rittby and R. J. Bartlett, An Open-Shell Spin-Restricted Coupled Cluster Method: Application to Ionization Potentials in N_2, *J. Phys. Chem.*, 1988, **92**, 3033–3036.

41 P. J. Knowles, C. Hampel and H.-J. Werner, Coupled Cluster Theory for High Spin, Open Shell Reference Wave Functions, *J. Chem. Phys.*, 1993, **99**, 5219–5228.

42 W. A. de Jong, R. J. Harrison and D. A. Dixon, Parallel Douglas-Kroll Energy and Gradients in NWChem: Estimating Scalar Relativistic Effects Using Douglas-Kroll Contracted Basis Sets, *J. Chem. Phys.*, 2001, **114**, 48–53.

43 J. L. Dunham, The Energy Levels of a Rotating Vibrator, *Phys. Rev.*, 1932, **41**, 721–731.

44 B. O. Roos, P. R. Taylor and P. E. Siegbahn, A Complete Active Space SCF Method (CASSCF) Using Density-matrix Formulated Super-CI Approach, *Chem. Phys.*, 1980, **48**, 157–173.

45 P. E. M. Siegbahn, J. Almlöf, A. Heiberg and B. O. Roos, The Complete Active Space SCF (CASSCF) Method in a Newton-Raphson Formulation with Application to the HNO Molecule, *J. Chem. Phys.*, 1981, **74**, 2384–2396.

46 H.-J. Werner, Matrix-Formulated Direct Multiconfiguration Self-Consistent Field and Multiconfiguration Reference Configuration-Interaction Methods, *Adv. Chem. Phys.*, 1987, 1.

47 H.-J. Werner and W. Meyer, A Quadratically Convergent Multiconfiguration-Self-Consistent Field Method with Simultaneous Optimization of Orbitals and CI Coefficients, *J. Chem. Phys.*, 1980, **73**, 2342–2356.

48 H.-J. Werner and W. Meyer, A Quadratically Convergent MCSCF Method for the Simultaneous Optimization of Several States, *J. Chem. Phys.*, 1981, **74**, 5794–5801.

49 N. B. Balabanov and K. A. Peterson, Systematically Convergent Basis Sets for Transition Metals. I. All-Electron Correlation Consistent Basis Sets for the 3d Elements Sc-Zn, *J. Chem. Phys.*, 2005, **123**, 064107.

50 H.-J. Werner, P. J. Knowles, G. Knizia, F. R. Manby and M. Schütz, Molpro: A General-Purpose Quantum Chemistry Program Package, *Wiley Interdiscip. Rev.: Comput. Mol. Sci.*, 2012, **2**, 242–253.

51 H.-J. Werner, P. J. Knowles, F. R. Manby, J. A. Black, K. Doll, A. Heßelmann, D. Kats, A. Köhn, T. Korona, D. A. Kreplin, Q. Ma, T. F. Miller III, A. Mitrushchenkov, K. A. Peterson, I. Polyak, G. Rauhut and M. Sibaev, The Molpro Quantum Chemistry Package, *J. Chem. Phys.*, 2020, **152**, 144107.

52 H.-J. Werner, P. J. Knowles, G. Knizia, F. R. Manby, M. Schütz, P. Celani, W. Györffy, D. Kats, T. Korona, R. Lindh, A. Mitrushenkov, G. Rauhut, K. R. Shamasundar, T. B. Adler, R. D. Amos, S. J. Bennie, A. Bernhardsson, A. Berning, D. L. Cooper, M. J. O. Deegan, A. J. Dobbyn, F. Eckert, E. Goll, C. Hampel, A. Hesselmann, G. Hetzer, T. Hrenar, G. Jansen, C. Köppl, S. J. R. Lee, Y. Liu, A. W. Lloyd, Q. Ma, R. A. Mata, A. J. May, S. J. McNicholas, W. Meyer, T. F. Miller III, M. E. Mura, A. Nicklass, D. P. O'Neill, P. Palmieri, D. Peng, T. Petrenko, K. Pflüger, R. Pitzer, M. Reiher, T. Shiozaki, H. Stoll, A. J. Stone, R. Tarroni, T. Thorsteinsson, M. Wang and M. Welborn, MOLPRO, version 2020.1, a package of ab initio programs, see **https://www.molpro.net**. [Accessed July 1, 2022].

53 E. R. Davidson and D. W. Silver, Size Consistency in the Dilute Helium Gas Electronic Structure, *Chem. Phys. Lett.*, 1977, **52**, 403–406.

54 K. Andersson, P. A. Malmqvist, B. O. Roos, A. J. Sadlej and K. Wolinski, Second-Order Perturbation Theory with a CASSCF Reference Function, *J. Phys. Chem.*, 1990, **94**, 5483–5488.

55 K. Andersson, P. A. Malmqvist, B. O. Roos, A. J. Sadlej and K. Wolinski, Second-Order Perturbation Theory with a

This journal is © the Owner Societies 2024

Phys. Chem. Chem. Phys., 2024, **26**, 19646–19657 | **19655**

Complete Active Space Self-Consistent Field Reference Function, *J. Chem. Phys*, 1992, **96**, 1218–1226.

56 D. A. Dixon, D. Feller and K. A. Peterson, A Practical Guide to Reliable First Principles Computational Thermochemistry Predictions Across the Periodic Table, in *Annual Reports in Computational Chemistry*, ed R. A. Wheeler, Elsevier, Amsterdam, 2012, vol. 8, ch. 1, pp. 1–28.

57 D. Feller, K. A. Peterson and D. A. Dixon, Further Benchmarks of a Composite, Convergent, Statistically-Calibrated Coupled Cluster-Based Approach for Thermochemical and Spectroscopic Studies, *Mol. Phys.*, 2012, **110**, 2381–2399.

58 K. A. Peterson, D. Feller and D. A. Dixon, Chemical Accuracy in *Ab Initio* Thermochemistry and Spectroscopy: Current Strategies and Future Challenges, *Theor. Chem. Acc.*, 2012, **131**, 1079.

59 D. Feller, K. A. Peterson and D. A. Dixon, The Impact of Larger Basis Sets and Explicitly Correlated Coupled Cluster Theory on the Feller-Peterson-Dixon Composite Method. in *Annual Reports in Computational Chemistry*, ed. D. A. Dixon, Elsevier, Amsterdam, 2016, vol. 12, pp. 47–78.

60 A. D. Becke, Density-Functional Thermochemistry. IV. A new Dynamical Correlation Functional and Implications for Exact-Exchange Mixing, *J. Chem. Phys.*, 1996, **104**, 1040–1046.

61 C. Adamo and V. Barone, Toward Reliable Adiabatic Connection Models Free from Adjustable Parameters, *Chem. Phys. Lett.*, 1997, **274**, 242–250.

62 J. P. Perdew, Density-Functional Approximation for the Correlation Energy of the Inhomogeneous Electron Gas, *Phys. Rev. B*, 1986, **33**, 8822–8824.

63 J. P. Perdew and Y. Wang, Accurate and Simple Analytic Representation of the Electron Gas Correlation Energy, *Phys. Rev. B*, 1992, **45**, 13244–13249.

64 A. D. Boese and N. C. Handy, New Exchange–Correlation Density Functionals: The Role of the Kinetic-Energy Density, *J. Chem. Phys.*, 2002, **116**, 9559–9969.

65 P. J. Wilson, T. J. Bradley and D. J. Tozer, Hybrid Exchange–Correlation Functional Determined from Thermochemical Data and *Ab Initio* Potentials, *J. Chem. Phys.*, 2001, **115**, 9233–9242.

66 H. L. Schmider and A. D. Becke, Optimized Density Functionals from the Extended G2 Test Set, *J. Chem. Phys*, 1998, **108**, 9624–9631.

67 A. D. Becke, Density-Functional Exchange-Energy Approximation with Correct Asymptotic Behavior, *Phys. Rev. A*, 1988, **38**, 3098–3100.

68 A. D. Boese and J. M. L. Martin, Development of Density Functionals for Thermochemical Kinetics, *J. Chem. Phys.*, 2004, **121**, 3405–3416.

69 T. Yanai, D. Tew and N. Handy, A New Hybrid Exchange–Correlation Functional Using the Coulomb-Attenuating Method (CAM-B3LYP), *Chem. Phys. Lett.*, 2004, **393**, 51–57.

70 J. Heyd, G. E. Scuseria and M. Ernzerhof, Hybrid Functionals Based on a Screened Coulomb Potential, *J. Chem. Phys.*, 2003, **118**, 8207–8215.

71 J. Heyd, G. E. Scuseria and M. Ernzerhof. Erratum: Hybrid functionals based on a screened Coulomb potential, *J. Chem. Phys.* 118, 8207, 2003.

72 J. Heyd and G. E. Scuseria, Assessment and Validation of a Screened Coulomb Hybrid Density Functional, *J. Chem. Phys.*, 2004, **120**, 7274–7280.

73 J. Heyd, J. E. Peralta, G. E. Scuseria and R. L. Martin, Energy Band Gaps and Lattice Parameters Evaluated with the Heyd–Scuseria–Ernzerhof Screened Hybrid Functional, *J. Chem. Phys.*, 2005, **123**, 174101.

74 A. V. Krukau, O. A. Vydrov, A. F. Izmaylov and G. E. Scuseria, Influence of the Exchange Screening Parameter on the Performance of Screened Hybrid Functionals, *J. Chem. Phys*, 2006, **125**, 224106.

75 O. A. Vydrov and G. E. Scuseria, Assessment of a Long Range Corrected Hybrid Functional, *J. Chem. Phys*, 2006, **125**, 234109.

76 Y. Zhao, N. E. Schultz and D. G. Truhlar, Design of Density Functionals by Combining the Method of Constraint Satisfaction with Parametrization for Thermochemistry, Thermochemical Kinetics, and Noncovalent Interactions, *J. Chem. Theory Comput.*, 2006, **2**, 364–382.

77 Y. Zhao, N. E. Schultz and D. G. Truhlar, Exchange–Correlation Functional with Broad Accuracy for Metallic and Nonmetallic Compounds, Kinetics, and Noncovalent Interactions, *J. Chem. Phys*, 2005, **123**, 161103.

78 Y. Zhao and D. G. Truhlar, The M06 suite of Density Functionals for Main Group Thermochemistry, Thermochemical Kinetics, Noncovalent Interactions, Excited States, and Transition Elements: Two New Functionals and Systematic Testing of Four M06-class Functionals and 12 Other Functionals, *Theor. Chem. Acc.*, 2008, **120**, 215–241.

79 Y. Zhao and D. G. Truhlar, Comparative DFT Study of van der Waals Complexes: Rare-Gas Dimers, Alkaline-Earth Dimers, Zinc Dimer, and Zinc-Rare-Gas Dimers, *J. Phys. Chem. A*, 2006, **110**, 5121–5129.

80 Y. Zhao and D. G. Truhlar, Density Functional for Spectroscopy: No Long-Range Self-Interaction Error, Good Performance for Rydberg and Charge-Transfer States, and Better Performance on Average than B3LYP for Ground States, *J. Phys. Chem. A*, 2006, **110**, 13126–13130.

81 Y. Zhao and D. G. Truhlar, Exploring the Limit of Accuracy of the Global Hybrid Meta Density Functional for Main-Group Thermochemistry, Kinetics, and Noncovalent Interactions, *J. Chem. Theory Comput.*, 2008, **4**, 1849–1868.

82 R. Peverati and D. G. Truhlar, Improving the Accuracy of Hybrid Meta-GGA Density Functionals by Range Separation, *J. Phys. Chem. Lett.*, 2011, **2**, 2810–2817.

83 R. Peverati and D. G. Truhlar, Screened-Exchange Density Functionals with Broad Accuracy for Chemistry and Solid State Physics, *Phys. Chem. Chem. Phys.*, 2012, **14**, 16187–16191.

84 H. S. Yu, X. He, S. L. Li and D. G. Truhlar, MN15: A Kohn–Sham Global-Hybrid Exchange–Correlation Density Functional with Broad Accuracy for Multi-Reference and Single-Reference Systems and Noncovalent Interactions, *Chem. Sci.*, 2016, **7**, 5032–5051.

85 C. Adamo and V. Barone, Exchange Functionals with Improved Long-Range Behavior and Adiabatic Connection Methods without Adjustable Parameters: The mPW and mPW1PW models, *J. Chem. Phys.*, 1998, **108**, 664–675.

19656 | *Phys. Chem. Chem. Phys.*, 2024, **26**, 19646–19657

This journal is © the Owner Societies 2024

86 J. P. Perdew, K. Burke and M. Ernzerhof, Generalized Gradient Approximation Made Simple, *Phys. Rev. Lett.*, 1996, **77**, 3865–3868.

87 J. P. Perdew, K. Burke and M. Ernzerhof, Erratum: Generalized Gradient Approximation Made Simple, *Phys. Rev. Lett.*, 1996, **77**, 3865.

88 A. J. Cohen and N. C. Handy, Dynamic Correlation, *Mol. Phys.*, 2001, **99**, 607–615.

89 C. Adamo and V. Barone, Toward Reliable Density Functional Methods Without Adjustable Parameters: The PBE0 model, *J. Chem. Phys.*, 1999, **110**, 6158–6169.

90 M. Ernzerhof and J. P. Perdew, Generalized Gradient Approximation to the Angle- and Aystem-Averaged Exchange Hole, *J. Chem. Phys.*, 1998, **109**, 3313–3320.

91 K. Burke, J. P. Perdew and Y. Wang, Derivation of a Generalized Gradient Approximation: The PW91 Density Functional, in *Electronic Density Functional Theory: Recent Progress and New Directions*, ed. J. F. Dobson, G. Vignale and M. P. Das, Springer, NY, 1998, pp. 81–111.

92 R. Peverati and D. G. Truhlar, A Global Hybrid Generalized Gradient Approximation to the Exchange–Correlation Functional That Satisfies the Second-Order Density-Gradient Constraint and Has Broad Applicability in Chemistry, *J. Chem. Phys.*, 2011, **135**, 191102.

93 J. C. Slater, *Quantum Theory of Molecules and Solids*, McGraw-Hill, New York, 1974, vol. 4.

94 S. H. Vosko, L. Wilk and M. Nusair, Accurate Spin-Dependent Electron Liquid Correlation Energies for Local Spin Density Calculations: A Critical Analysis, *Can. J. Phys.*, 1980, **58**, 1200–1211.

95 A. D. Boese and N. C. Handy, New Exchange–Correlation Density Functionals: The Role of the Kinetic-Energy Density, *J. Chem. Phys.*, 2002, **116**, 9559–9969.

96 V. N. Staroverov, G. E. Scuseria, J. Tao and J. P. Perdew, Comparative Assessment of a New Nonempirical Density Functional: Molecules and Hydrogen-Bonded Complexes, *J. Chem. Phys.*, 2003, **119**, 12129–12137.

97 J.-D. Chai and M. Head-Gordon, Systematic Optimization of Long-Range Corrected Hybrid Density Functionals, *J. Chem. Phys.*, 2008, **128**, 084106.

98 J.-D. Chai and M. Head-Gordon, Long-range Corrected Hybrid Density Functionals with Damped Atom-atom Dispersion Corrections, *Phys. Chem. Chem. Phys.*, 2008, **10**, 6615–6620.

99 J.-D. Chai and M. Head-Gordon, Systematic Optimization of Long-range Corrected Hybrid Density Functionals, *J. Chem. Phys*, 2008, **128**, 084106.

100 X. Xu and W. A. Goddard, The X3LYP Extended Density Functional for Accurate Descriptions of Nonbond Interactions, Spin States, and Thermochemical Properties, *Proc. Natl. Acad. Sci. U. S. A.*, 2004, **101**, 2673–2677.

101 A. E. Reed, L. A. Curtiss and F. Weinhold, Intermolecular Interactions from a Natural Bond Orbital, Donor–Acceptor Viewpoint, *Chem. Rev.*, 1988, **88**, 899–926.

102 F. Weinhold and C. R. Landis, *Valency and Bonding: A Natural Bond Orbital Donor–Acceptor Perspective*, University Press, Cambridge, U.K., 2005.

103 E. D. Glendening, J. K. Badenhoop, A. E. Reed, J. E. Carpenter, J. A. Bohmann, C. M. Morales, P. Karafiloglou, C. R. Landis and F. Weinhold, Natural Bond Order 7.0, Theoretical Chemistry Institute, University of Wisconsin, Madison, WI, 2018.

104 E. D. Glendening, C. R. Landis and F. Weinhold, NBO 7.0: New Vistas in Localized and Delocalized Chemical Bonding Theory, *J. Comput. Chem.*, 2019, **40**, 2234–2241.

105 M. J. Frisch, G. W. Trucks, H. B. Schlegel, G. E. Scuseria, M. A. Robb, J. R. Cheeseman, G. Scalmani, V. Barone, G. A. Petersson, H. Nakatsuji, X. Li, M. Caricato, A. V. Marenich, J. Bloino, B. G. Janesko, R. Gomperts, B. Mennucci, H. P. Hratchian, J. V. Ortiz, A. F. Izmaylov, J. L. Sonnenberg, D. Williams-Young, F. Ding, F. Lipparini, F. Egidi, J. Goings, B. Peng, A. Petrone, T. Henderson, D. Ranasinghe, V. G. Zakrzewski, J. Gao, N. Rega, G. Zheng, W. Liang, M. Hada, M. Ehara, K. Toyota, R. Fukuda, J. Hasegawa, M. Ishida, T. Nakajima, Y. Honda, O. Kitao, H. Nakai, T. Vreven, K. Throssell, J. A. Montgomery, Jr., J. E. Peralta, F. Ogliaro, M. J. Bearpark, J. J. Heyd, E. N. Brothers, K. N. Kudin, V. N. Staroverov, T. A. Keith, R. Kobayashi, J. Normand, K. Raghavachari, A. P. Rendell, J. C. Burant, S. S. Iyengar, J. Tomasi, M. Cossi, J. M. Millam, M. Klene, C. Adamo, R. Cammi, J. W. Ochterski, R. L. Martin, K. Morokuma, O. Farkas, J. B. Foresman and D. J. Fox, *Gaussian 16, Revision C.01*, Gaussian, Inc., Wallingford CT, 2016.

106 Z. Fang, J. Both, S. Li, S. Yue, E. Aprà, M. Keçeli, A. F. Wagner and D. A. Dixon, Benchmark Calculations of Energetic Properties of Groups 4 and 6 Transition Metal Oxide Nanoclusters Including Comparison to Density Functional Theory, *J. Chem. Theor. Comput.*, 2016, **12**, 3689–3710.

107 Z. Fang, Z. Lee, K. A. Peterson and D. A. Dixon, Use of Improved Orbitals for CCSD(T) Calculations for Predicting Heats of Formation of Group IV and Group VI Metal Oxide Monomers and Dimers and UCl6, *J. Chem. Theor. Comput.*, 2016, **12**, 3583–3592.

108 Z. Fang, M. Vasiliu, K. A. Peterson and D. A. Dixon, Prediction of Bond Dissociation Energies/Heats of Formation for Diatomic Transition Metal Compounds: CCSD(T) Works, *J. Chem. Theor. Comput.*, 2017, **13**, 1057–1066.

109 T. J. Lee and P. R. Taylor, A Diagnostic for Determining the Quality of Single-Reference Electron Correlation Methods, *Int. J. Quantum Chem. Symp.*, 1989, **23**, 199–207.

110 A. Kramida, Yu Ralchenko and J. Reader, NIST ASD Team (2023). NIST Atomic Spectra Database (ver. 5.11), [Online]. Available: **https://physics.nist.gov/asd** [2024, April 22]. National Institute of Standards and Technology, Gaithersburg, MD, DOI: **10.18434/T4W30F** (Accessed April 1, 2024).

111 U. Litzén, J. W. Brault and A. P. Thorn, Spectrum and Term System of Neutral Nickel, Ni I, *Phys. Scr.*, 1993, **47**, 628–673.

This journal is © the Owner Societies 2024

Phys. Chem. Chem. Phys., 2024, **26**, 19646–19657 | **19657**